The influence of high-porosity nickel foam on the transition flow regime for heat transfer and pressure drop characteristics in a rectangular channel

Sohaib Osman[1,2] · Mohsen Sharifpur[1,3] · Josua P. Meyer[1] · Lingen Chen[4]

Abstract

This study investigates an approach of enhancing heat transfer in heat exchangers by increasing heat transfer area of the heat exchanger, and this is done by filling the rectangular test section with porous media to extend the heat transfer surface area and thus enhance the heat transfer. The permeability of the used nickel foam is determined by conducting pressure drop measurements through the nickel foam in the test section, and the heat transfer and pressure drop parameters are measured and compared with the empty test section. The results show that the values of the friction coefficient are 24.5 times the values of the empty test section, and the Nusselt number is observed to be three times higher when using nickel foam than that without foam in the test section. No transition regime is observed for the foam-filled test section on both heat transfer and pressure drop results; however, the transition from laminar to turbulent is found for the test section without foam. The results of thermal factor of the foam-filled test section show a thermal performance factor higher than unity through the entire Reynolds number range of 2000–6500, with better thermal performance factor at lower Reynolds number.

Keywords Porous media · Nickel foam · Transition · Heat transfer enhancement · Rectangular channel

List of symbols

A_c	Cross-sectional area, (m^2)
A_S	Surface area, (m^2)
c_p	Specific heat, (J kg^{-1} K^{-1})
D_h	Hydraulic diameter, (m)
h	Heat transfer coefficient, (W m^{-2} K^{-1})
H	Height of the channel cross-section, (m)
$h(x)$	Local heat transfer coefficient, (W m^{-2} K^{-1})
k	Thermal conductivity, (W m^{-2} K^{-1})
L	Tube length, (m)
$\dot{m}$	Mass flow rate, (kg s^{-1})
$\frac{dP}{dx}$	Pressure gradient, (Pa m^{-1})
Q	Heat rate, (W)
$\dot{q}$	Heat flux, (W m^{-2})
T	Temperature
V	Flow velocity, (m s^{-1})
W	Channel depth, (m)

Greek symbols

α	Aspect ratio
μ	Dynamic viscosity, (Pa s)
ρ	Mass density, (kg m^{-3})
ΔP	Pressure drop, (Pa)

Non-dimensional numbers

Re	Reynolds number (Hydraulic diameter based)
Re$_K$	Permeability-based Reynolds number
Re*	Modified Reynolds number
Nu	Nusselt number
K	Permeability

Subscript

Avg.	Average
b	Bulk
b$_f$	Base fluid
e	Exit

✉ Mohsen Sharifpur
  mohsen.sharifpur@up.ac.za

✉ Lingen Chen
  lingenchen@hotmail.com

1   Department of Mechanical and Aeronautical Engineering, University of Pretoria, Private Bag X20, Pretoria 0028, South Africa

2   Mechanical Engineering Department, University of Khartoum, P.O. Box 321, Khartoum, Sudan

3   Department of Medical Research, China Medical University Hospital, China Medical University, Taichung, Taiwan

4   Institute of Thermal Science and Power Engineering, Wuhan Institute of Technology, Wuhan 430205, China

i   Inlet
f   Friction coefficient

Introduction

Metal foams are lightweight materials with an irregular cellular and porous structure, and metal foams can be split into open cell or closed cell. In the closed-cell metal foams, the cells form a stand-alone enclosure within the material, while in the open-cell metal foams, the cells are all interconnected with no walls permitting the fluid to pass with less pressure drop. The metal foams possess unique properties compared with the traditional porous media. However, not much research has been done on metal foams, while many studies reported on conventional porous media [1–6] and some books have also focused on porous media [7–9].

In the past few decades, several researchers have explored the uses of metallic foams in heat exchangers to reduce the size of heat exchangers in thermal management applications and to enhance heat transfer. Beavers and Sparrow [10] conducted the first study of metal foam. They studied the pressure drop across nickel foams without reporting the pore size and the porosity. The Reynolds number was evaluated based on the permeability. They found that the flow pattern deviated from the Darcy regime at unity Reynolds number. Paek et al. [11] determined the thermophysical properties of aluminium-based metal foams. The permeability and thermal conductivity of the foams were measured while air flowed through the metal foams. They found that permeability was influenced by the pore size and the porosity, while thermal conductivity increased when the porosity decreased and remained unaffected by the pore size. A correlation for the friction coefficient was developed as a function of permeability and inertial forces. Miwa and Revankar [12] developed an apparatus to investigate the permeability of metal foam. Various nickel foams with different pore sizes were used. The permeability of nickel foams was experimentally determined by measuring the pressure drop across the foam. A correlation was obtained for this type of metal foam in a Darcian flow regime. The developed friction factor correlation was a function of the Reynolds number based on the permeability as characteristic length and included the effects of the pore size and structure. Calmidi and Mahajan [13] found that heat transfer enhancement was very low for aluminium foam when the working fluid was air, while water enhanced the forced convection heat transfer considerably. Kim et al. [14] studied the effect of metal foam permeability on Nusselt number and friction coefficients, and testing results on aluminium foams revealed that the low permeable foams resulted in a high Nusselt number, but high friction factors were noticed. Nazari et al. [15] studied the heat transfer and pressure drop characteristics

of Al$_2$O$_3$-water nanofluids flowing in a horizontal circular pipe packed with metal foam and compared the results with those of the empty tube. The results of the porous media test section showed remarkable enhancement of heat transfer compared with those of the empty tube with a penalty in the pressure drop. A maximum increase in "Nusselt number" of 57% was achieved. Noh et al. [16] conducted an experiment on an annulus filled with aluminium foam and obtained pressure drop, average and local convective heat transfer. The non-Darcy flow in the metal foam showed enhancement in the laminar flow regime compared with the empty annulus. The correlation for friction coefficient and heat transfer was developed to suit the tube-in-tube and shell-in-tube heat exchangers and was used in the design phase for these heat exchangers. Wang and Guo [17] investigated the pressure drop and the heat transfer performance of stainless steel metal foam. Three different pore sizes were manufactured using the sintering technique, and the pressure drop of air flowing at high speed was measured. Compared with the low-speed airflow correlations, the pressure drop was found to be highly dominated by inertial drag. The Nusselt numbers data were obtained under the convective boundary conditions and found to be higher than the values of the reported Nusselt number under constant heat flux condition.

Mancin et al. [18] investigated the effect the foam height on the heat transfer coefficient and the pressure gradient of air flowing in two different aluminium foam with same porosity but different height, the heat flux was also changed, and the results revealed that the heat flux has no effect on the heat transfer while increasing the foam height has a reverse impact on the heat transfer, and the pressure drop was remained unchanged with the foam height. Hamadouche et al. [19] considered the heat transfer enhancement of a foam-filled channel, which was filled with aluminium foam. The study reported that the heat transfer of air flowing through aluminium foam in the turbulent regime was 300% higher than in the empty channel. Dukhan et al. [20] investigated flow regime in a metal foam consisting of an aluminium foam pore density of 20 pores per inch and a porosity of 87.6%. A set of points were measured to plot the friction coefficient of the foam with Reynolds number, and the square root of the permeability was considered as a characteristic length to evaluate Reynolds number. The transition from pre-Darcy to turbulent flow was investigated and compared with the transition in the traditional porous media found in the literature. The study showed that the permeability and inertial drag coefficient values were different in the various flow regimes for the same foam.

The type of metal foam used in this research falls under the group of the open-cell metal foams and is a porous media with high porosity and the following interesting properties [9]: (a) lightweight because of the high number of voids in the foam, (b) high specific surface area, which leads to compact heat

exchanger design, (c) machinability and weldability to facilitate the formation of the complex parts, and (d) excellent fluid mixing, which enhances the heat transfer rate.

From the above-reviewed literature, it is clear that the high-porosity metal foams were not investigated enough in terms of heat transfer enhancement, and this paper is an attempt to understand the heat transfer capabilities of this kind of foam. It also fills the knowledge gap on the pressure drop and heat transfer compared to the empty test section.

Experimental methods

Test section building procedures

Initially, a rectangular test section is procures with the specification as listed in Table 1.The test section is filled with a porous media insert of rectangular shape to assist in the heat transfer enhancement by increasing the contact surface area with the channel. The porous media is high-porosity foam procured from Alantum, Korea. The supplied foam is initially a rectangular sheet of 200×300 mm. The standard specification of the nickel foam is given by the supplier (Alantum) and listed in Table 2. The foam is cut into strips with the same dimensions as those of the test section to place it in the test section. Figure 1 shows the foam strips placed in the rectangular channel.

The strips are cut accurately to the required size by using water jet cutting technology; the strip height is made to be slightly higher than the channel height to produce strong, tight bonding with the channel. The dimensions of the cut foam and the open channel are illustrated in Fig. 2a, and the placement of the foam in the channel before and after mechanical bonding of the top of the channel is shown in Fig. 2b and c, respectively.

For the placement of the nickel porous foam in the test section, the top of the channel is opened, as shown in Fig. 1 by using a bench saw, and then the top is machined to ensure a smooth surface to assist bonding the top of the channel to the test section, and then the foam is placed along the channel length by mechanical bonding, as shown in Fig. 3a. To secure the foam inside the channel, the plate is also brazed carefully, as shown in Fig. 3b, to avoid any solder droplet to leak into the channel, preventing the clogging of porous media, and preventing any leaks of the nanofluids while testing. The porosity of the foam-filled test section is determined experimentally to count for any changes occurring to the porous media because of the foam insertion process to the channel. It is determined

Table 1 Standard specification of the empty rectangular channel

Width/mm	Depth/mm	Thickness	Material
10	7	1 mm	Copper

Table 2 Standard specification for the Ni foam supplied by alantum

Pore size/mm	Area density/g mm^{-2}	Porosity/%	Thickness/mm
3	800	98	3.5

by measuring the volume of the water inside the foam test section and then divide it by the volume of the water that filled the test section. The porosity is found to be 3% less than the original foam porosity, and this value is considered for the calculation.
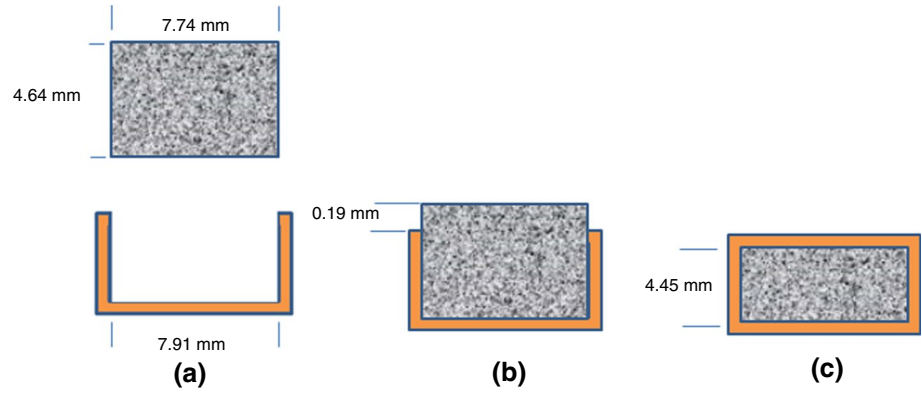
Description of the experimental set-up

The testing rig is designed and constructed to facilitate the measurements of the convective heat transfer and the pressure drop for the nanofluids. Figure 4 displays the general circulation loop of the test rig as it consists of supply tank (1) from which the magnetic variable speed pump (2) takes the fluid and circulate it to the test Sect. 3. 200 W DC power supply is used to heat the test section. A heating element is winded around the test section to enable the uniform heat flux application. The test section is coated by thermal insulation (4) of 50 mm thick (four layers) to reduce the heat losses from the heating coil to the surroundings. The fluid exits the test section at a higher temperature to the flow meter (5). The hot fluid needs to be cooled down in a separate cooling loop. The cooling loop gets cold water from a chiller (6), and then the cold water circulates through the cold water circulating pump (7) to the shell and tube heat exchanger (8), in which the hot fluid cooled and was supplied to the rectangular channel again at (20 °C). A Data Acquisition (DAQ) system is used to process the electrical signals from the thermocouples, pressure transducers, flow meters and the power supply and then dispatches them to the data capturing program display (9). Measured parameters of the experiments are monitored through the Lab View program. A detailed description of the test section configuration
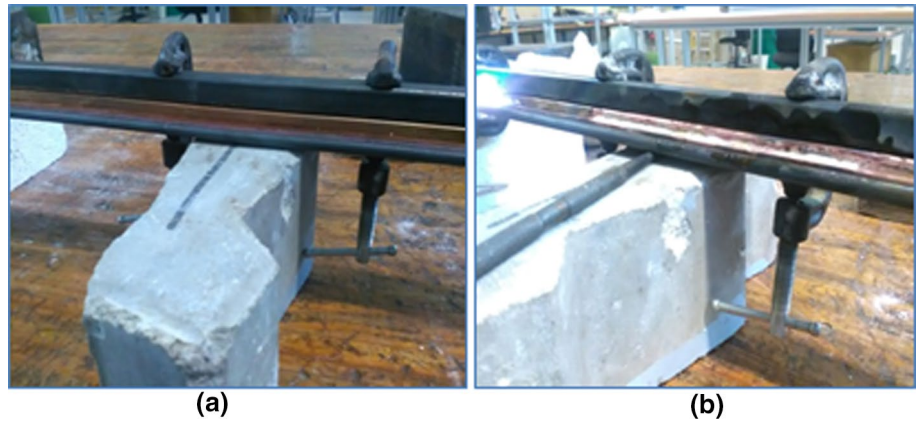

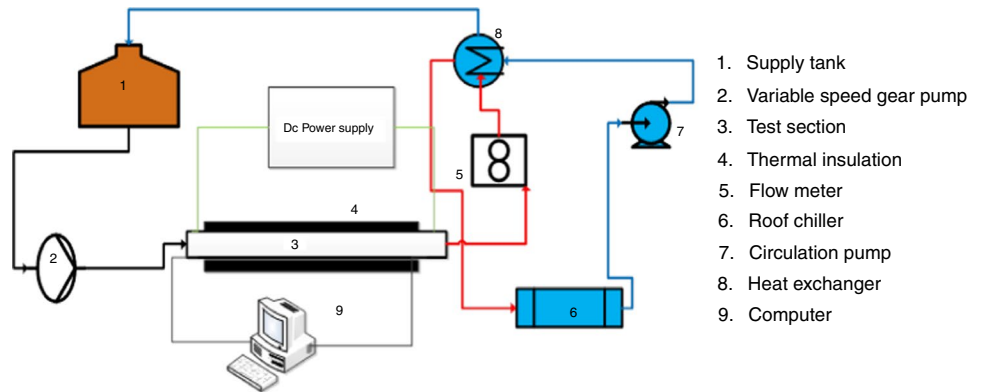**Fig. 1** Nickel foam placement in the open rectangular channel

Fig. 2 a Top opened test section and the foam, **b** foam inserted tightly into the test section, **c** foam mechanically ponded to the test section after the top of the test section was brazed

Fig. 3 a Mechanical ponding of the foam and the test section, **b** brazing of the top of the channel

Fig. 4 Schematic diagram of the of the experimental setup circulation loop

1. Supply tank
2. Variable speed gear pump
3. Test section
4. Thermal insulation
5. Flow meter
6. Roof chiller
7. Circulation pump
8. Heat exchanger
9. Computer

and setup was presented in the work of Osman et al. [21]. The connection of the test section to the test rig and the details of the thermocouples distribution are shown in Fig. 5
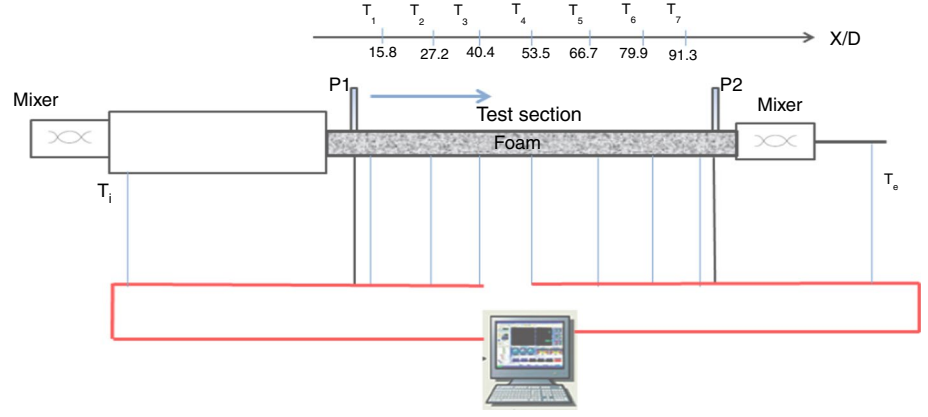
Mathematical formulation

Friction coefficient

The average flow velocity (V) can be obtained from the equation:

$$V = \frac{\dot{m}}{\rho A_{c}} \tag{1}$$

Fig. 5 Schematic of the nickel foam inserted in the test section, and the thermocouple stations distribution

The hydraulic diameter is calculated using the formula:

$$D_h = \frac{4WH}{2W + 2H} \tag{2}$$

where H and W are the height and the depth of the rectangular cross-section, respectively.

To estimate the friction coefficient, Darcy equation is used:

$$f = \frac{2\Delta P D_h}{\rho L V^2} \tag{3}$$

Nusselt number

The amount of heat transferred to the water (Q_{Water}) is found using the following expression:

$$\dot{Q}_{water} = \dot{m} \cdot c_p \cdot \left(T_e - T_i\right) \tag{4}$$

The heat flux ($\dot{q}$) is given as:

$$\dot{q} = \frac{\dot{Q}_{water}}{A_s} \tag{5}$$

The area where heat transfer occurred is:

$$A_s = (2W + 2H)L \tag{6}$$

The distribution of the mean temperature is calculated as follows:

$$T_m(x) = T_i + \frac{\dot{q}x(2W + 2H)}{\dot{m}c_p} \tag{7}$$

The following formula is considered for local heat transfer coefficient:

$$h(x) = \frac{\dot{q}}{\left[T_{wi}(x) - T_m(x)\right]} \tag{8}$$

The Nusselt number is found as follows

$$Nu = \frac{h_{avg}D_h}{k} \tag{9}$$

The Reynolds number is determined by:

$$Re = \frac{\rho V D_h}{\mu} \tag{10}$$

Permeability of the nickel foam

The relation between the pressure distribution across the porous media and flow velocity [7] can be found from Eq. (14) as follows:

$$\frac{dp}{dx} = \frac{\mu}{K}V + \frac{C_E}{\sqrt{K}}\rho V^2 \tag{11}$$

where K is the permeability, and it varies with the geometrical characteristic of the porous media. For the high fluid velocity, the inertial effect is dominant, and the flow range is known as the non-Darcy flow regime. The flow range in the test section under investigation falls under the non-Darcy flow regime. Therefore, it is necessary to calculate the permeability of the nickel foam that is inserted into the rectangular test section. Equation (12) is a reformulation of Eq. (11) for the purpose of the linearization of the equation:

$$\frac{1}{\mu V}\left(\frac{dp}{dx}\right) = \frac{1}{K} + \frac{C_E}{\sqrt{K}}\frac{\rho V}{\mu} \tag{12}$$

A common way to write Reynolds number is to define $\sqrt{K}$ as characteristic length, as follows [7]:

5

$$\mathrm{Re} = \frac{\rho V \sqrt{K}}{\mu} \tag{13}$$

The friction coefficient is calculated by the measurements of the pressure drop using Eq. (14)

$$f = \frac{\Delta P D_{\mathrm{h}}}{\rho L V^2} \tag{14}$$

Uncertainty analyses

The uncertainties are evaluated for the calculated and measured parameters by following the method recommended by Dunn [22]. The method uses linear regression analysis to determine the bias of the thermocouples, pressure transducers, and flow meters to determine a mathematical relation between two or more variables. The results of the uncertainties for the used instruments as well as the calculated parameters are calculated and presented in Tables 3 and 4, respectively.

Results and discussion

Validation of experimental set-up

The testing rig is validated against the available data in the literature by comparing the obtained experimental data of the pure water with well-established correlations in the turbulent and laminar flow regimes. The friction coefficient and Nusselt number are determined for pure water and compared with the correlations.

Validation of the adiabatic friction coefficients

The adiabatic friction coefficients are calculated by measuring the pressure drop across the test. Leon and Roman [23] developed correlations for the friction factor in the laminar and turbulent regimes as shown in Eqs. (15) and (16), respectively:

Table 3 Ranges and accuracies of instruments used

Instrument	Range	Uncertainty
Thermocouples	− 200–350 °C	0.1 °C
Coriolis flow meter	0–0.07 kg/s	0.1%
Pressure transducers	0–17 kPa	0.16%
Power supply	0–320 V	0.33 V
	0–12.5 V	0.04 A

Table 4 Uncertainties of the calculated parameters

	Re/%	ΔP/%	f/%	h/%	Nu/%
Re (high)	5	1	1	5	5
Re (low)	5	17	17	1	2

$$f_{\mathrm{lamiar}} = \frac{64}{\mathrm{Re}^*} \tag{15}$$

$$f_{\mathrm{turbulent}} = 0.316 \left(\mathrm{Re}^*\right)^{-0.25} \tag{16}$$

The two correlations are corrected by introducing a modified Reynolds number to the classical Poiseuille [24], and Blasius [25] correlations to be suitable for the rectangular cross-section channels. The correlations are used to validate the measured data.

The modified Reynolds number (Re^*) is calculated as follows:

$$\mathrm{Re}^* = \frac{\mathrm{Re}}{2\left(\frac{W}{H}\right)^{0.16}} \tag{17}$$

The measured laminar friction factor is compared to the prediction by the laminar correlation of Leon and Roman [23] as presented in Fig. 6. The comparison results yield an excellent agreement between the measurements and the prediction as the average deviation was 1.7%. On the other hand, as presented in Fig. 6, the comparison in the turbulent side reveals a good agreement with Leon and Roman (Turbulent) [23], as the difference is less than 1.3% throughout the turbulent region.
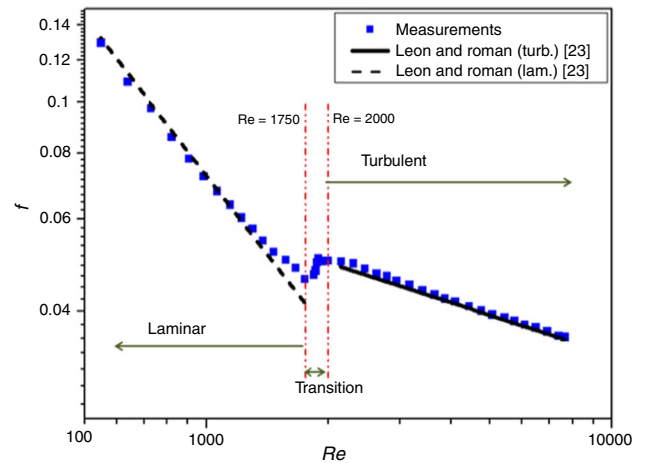
Fig. 6 Comparison of measured data of the adiabatic friction coefficient to the correlations (logarithmic scale)
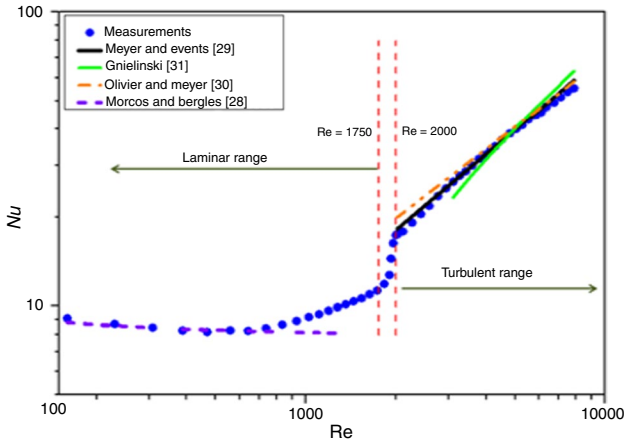
Fig. 7 Comparison of Nusselt number results to the correlations in laminar and turbulent regimes (logarithmic scale)

Fig. 8 Linear relation of pressure gradient across the porous media with the velocity

From Figs. 6 and 7, important observations are noticed, the transition starts at Reynolds number of 1750 and ends at 2000. The length of the transition is found to be 250 Reynolds number. Moreover, the standard critical Reynolds number where transition starts in circular tubes is at 2300 [26]. The observed early transition in rectangular channels as shown in Figs. 6 and 7 can be attributed to the cross-section of the channel as well as the inlet shape [27].

Validation of heat transfer measurements

Correlation of Morcos and Bergles [28] is used to validate Nusselt number data in the laminar regime, and the average deviation between the prediction and the measurements is 0.7% as shown in Fig. 7. Three correlations are used in the turbulent zone; average Nusselt number matches well with the Everts and Meyer [29], the measurements deviate by 1.8%. The correlation of Olivier and Meyer [30] is found to be higher than the measured values by an average of 3.8%. Gnielinski correlation [31] under-predicts the measurements reasonably well by 6% in the range of Reynolds numbers of 3000–5000, and over-predicts the data by 7% in the range of Reynolds numbers greater than 5000. Both Olivier and Meyer [30] and Gnielinski [31] correlations are not accurate enough to estimate the Nusselt number on the region between Reynolds numbers of 2000 and 3000, as they under-predicts the data by 12 and 21%, respectively. The reason behind the notable deviation is that the two correlations are generated to estimate the turbulent regime where the Reynolds numbers is higher than 3000.
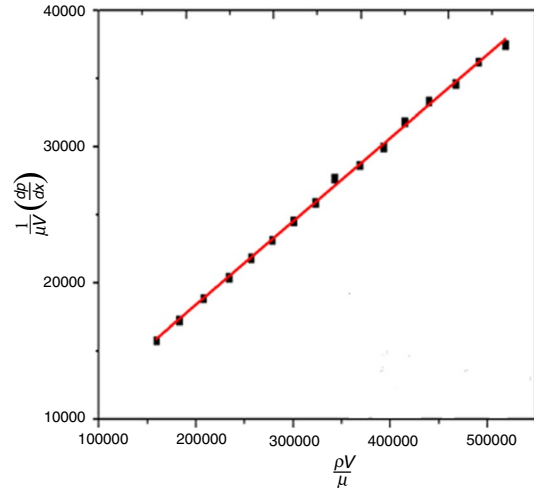
Hydrodynamic and heat transfer characteristics of the porous media insert

Hydrodynamic and permeability of the nickel foam

Figure 8 shows the linear relation between $\frac{1}{\mu V}\left(\frac{dp}{dx}\right)$ and $\frac{\rho V}{\mu}$ as observed from Eqs. (14) and (15). The values of the permeability (K) and Ergun coefficient (C_E) are extracted from the figure and are 0.000162 and 0.00078, respectively.

The friction coefficient variation with the Reynolds number for the test section with the nickel foam insert is shown
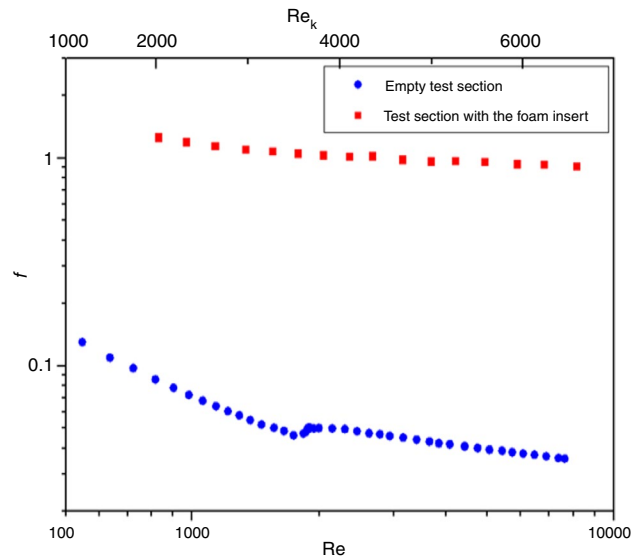

Fig. 9 Comparison of the friction coefficient variation with Reynolds number of the empty and nickel foam insert channel (logarithmic scale)

7

in Fig. 9. The permeability-based Reynolds number span ranges between 2000 and 6500. The range corresponds to the full flow range in the empty test section (laminar to turbulent, including the transition regime). The friction coefficient of the foam-filled test section shows no change in the pattern of the measurements, which indicates no transition, and the flow regime followed the non-Darcy flow regime. Moreover, the values of the friction coefficient are significantly higher than those for the empty test section value (24.5 times higher than the values of the empty test section), and this can be explained by the complicated structure of the nickel foam resulting in a flow fouling and therefore high pressure drop through the test section.

Heat transfer evaluation of the test section with the nickel foam insert

The variations of the local Nusselt number for two Reynolds numbers at seven various positions along the test section are presented in Fig. 10. For both Reynolds numbers (higher and lower), the Nusselt number decreases until the value of $x/D_h = 30$, which corresponds to the entrance length, where the flow is still thermally developing. These results indicate no effect of the foam in the thermal entrance length compared with the empty test section. The Nusselt number for the $Re = 8400$ is unchanged throughout the remaining segment of the test section, while the Nusselt number at Reynolds number of 1710 increases with the length of the tube, and it is 2.7 times higher than the value of Nusselt number at the position of $x/d = 30$. Figure 11 shows the average Nusselt number variation with Reynolds number for the water flow across the nickel foam in the rectangular channel. The comparison results with the empty test section show that a drastic increase in Nusselt number is observed
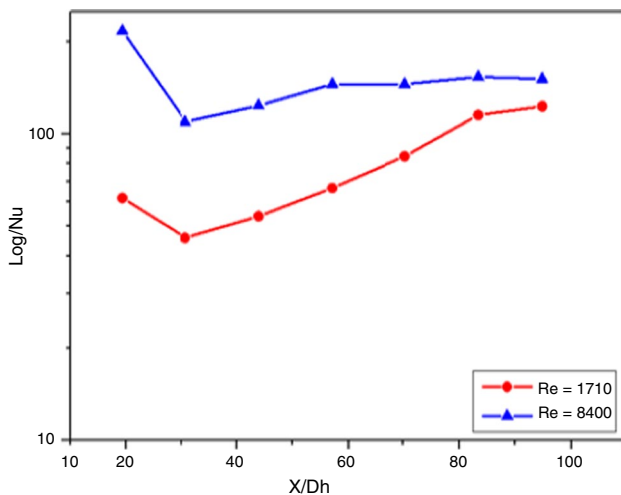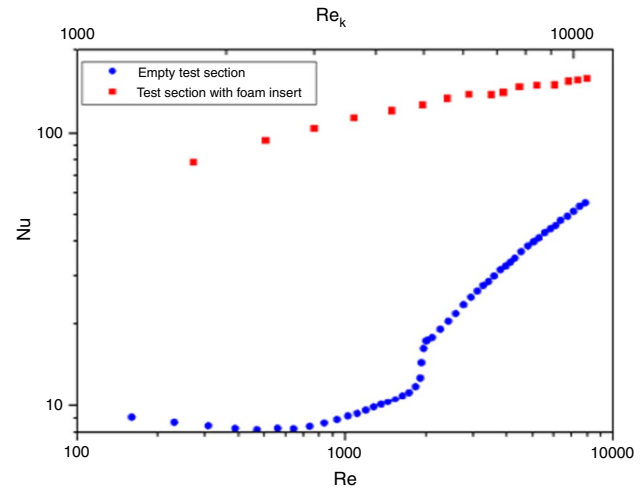

Fig. 11 Nusselt number comparison of flow through an empty rectangular test section and nickel foam inserted test section (logarithmic scale)

by using the nickel foam, whereas the increase is three times on average compared with that of the empty test section. The Nusselt number for the foam-filled test section increases with a higher rate in lower Reynolds number, a 77% increase for the range of Reynolds number between 1700 and 6000 is observed, while the increase in Nusselt number for the higher Reynolds number range (6000–10,000) is as little as 13%. This result can be justified by inspecting the behaviour of local heat transfer for the higher and low flow rate, as illustrated in Fig. 10, because the increment in the Nusselt number is almost negligible at the higher Reynolds number compared with the lower Reynolds number. Another feature demonstrated in Fig. 11 is the one pattern of Nusselt number variation with Reynolds number because no transition is noticed in the tested flow range. The transition from the laminar to turbulent is observed for the flow in the empty test section at Reynolds number of 1750 and ended at Reynolds number of 2000. This shows the effect of the porous media on the transition because no transition occurred when inserting the nickel foam in the rectangular test section.

It is noticed that the local Nusselt number is getting steady towards the exit of the test section, and this could be justified due to the fact that at the exit, the flow will be thermally developed. In contrast, it will be still developing at the entry of the test section.

Heat transfer enhancement evaluation of the nickel foam test section

The thermal performance factor is used as heat transfer enhancement criteria, as stated in Eq. (18), to compare the

Fig. 10 Local Nusselt number of two different flow rates through nickel foam in a rectangular test section
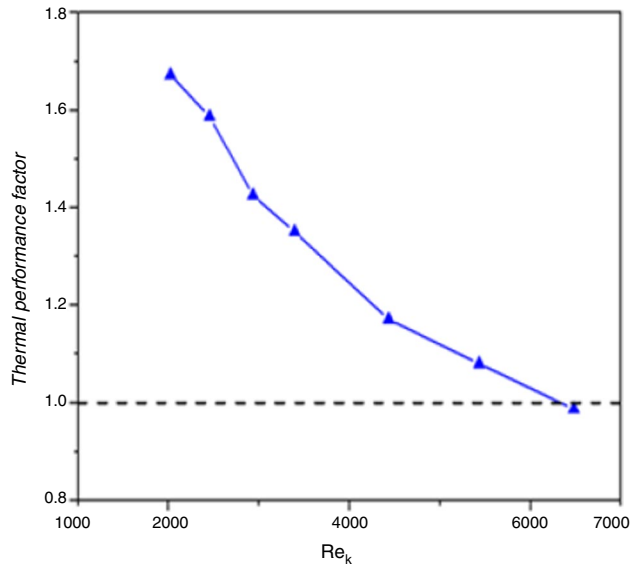
Fig. 12 Thermal performance coefficient relationship with Reynolds number for flow through a rectangular channel filled with nickel foam

obtained heat transfer enhancement with the penalty in the pressure drop.

$$\text{Thermal performance factor} = \frac{\frac{\text{Nu}_{\text{foam}}}{\text{Nu}_{\text{empty}}}}{\left(\frac{f_{\text{foam}}}{f_{\text{empty}}}\right)^{1/3}} \quad (18)$$

where Nu_{foam} and Nu_f are the Nusselt number of the water flowing through the foam-filled and the empty test sections, respectively, while f_{foam} and f_f are the friction coefficients in the foam-filled and the empty test sections, respectively.

Figure 12 shows that the thermal performance factor is higher than the unity through the entire tested Reynolds number range. This could be referred to the increasing in the heat transfer area caused by the foam insert as it acts as fins extended from the internal surfaces of the channel. Moreover, the open cell structure of the foam will help to mix the flow and cutting the boundary layer leading to uniform temperature distribution, and hence enhancement in the heat transfer compared to the test section. The higher performance factor values prove the feasibility of using the nickel foam as a method of heat transfer enhancement, although the high-pressure drop occurs when using the foam. The results also reveal that the operation of the foam-filled rectangular test section is better than at the lower flow rates because the thermal performance factor is observed to be 1.7.

Conclusions

The foam-filled test section is constructed by ponding the foam strips to the channel, and the permeability is determined by linearizing the no-Darcy flow pressure gradient equation. The pressure drop for the foam test section is 24.5 times higher than for the empty test section. However, the Nusselt number shows an increase of three times the empty test section value. The overall thermal performance factor shows the effectiveness of filling the test section with high-porosity nickel foam. No transition regime is noticed for the foam-filled test section on both the heat transfer and hydrodynamic results, while the transition from laminar to turbulent is spotted for the empty test section. The following highlights are also observed and concluded:

- A higher pressure drop when using the nickel foam is observed than when using the empty channel.
- The local heat transfer coefficients for the test section filled with the nickel foam shows that the thermal entry length does not depend on the flow rate.
- The heat transfer increment is constant towards the exit of the rectangular channel at the higher flow rates, while it increases rapidly at the lower flow rates.
- Nusselt numbers for the foam-filled test are above those for the empty test section indicating a heat transfer improvement when using nickel foam.
- No transition regime is noticed for the foam-filled test section on either the heat transfer results or the pressure drop results, while the transition from laminar to turbulent is observed for the empty test section.

Author Statement SO was involved in conceptualization, methodology, validation, writing—original draft preparation. MS was involved in conceptualization, validation, data curation, writing—reviewing and editing. JPM was involved in validation, data curation, writing—reviewing and editing. LC was involved in conceptualization, supervision, writing—reviewing and editing

References

1. Seguin D, Montillet A, Comiti J, Huet F. Experimental characterization of flow regimes in various porous media-II: Transition to turbulent regime. Chem Eng Sci. 1998; 53(22), 3897–909.

2. Seguin D, Montillet A, Comiti J. Experimental characterisation of flow regimes in various porous media-I: Limit of laminar flow regime. Chem Eng Sci. 1998; 53(21), 3751–61.

3. Rode S, Midoux N, Latifi MA, Storck A, Saatdjian E. Hydrodynamics of liquid flow in packed beds: an experimental study using electrochemical shear rate sensors. Chem Eng Sci. 1994; 49(6), 889–900.

4. Kececioglu I, Jiang Y. Flow through porous media of packed spheres saturated with water. J Fluids Eng. 1994;116(1):164–70.

5. Fand RM, Kim BYK, Lam ACC, Phan RT. Resistance to the flow of fluids through simple and complex porous media whose matrices are composed of randomly packed spheres. J Fluids Eng. 1987;109(3):268–73.

6. Dybbs A, Edwards RV. A New Look at Porous Media Fluid Mechanics—Darcy to Turbulent. In: Bear J, Corapcioglu MY, editors. Fundamentals of Transport Phenomena in Porous Media. Dordrecht: Springer, Netherlands; 1984. p. 199–256.

7. Nield DA, BejanA. Convection in Porous Media, 4th edn. Springer, Heidelberg, 2013.

8. Bear J. Dynamics of Fluids in Porous Media. American Elsevier Company, 1972.

9. T'Joen C., De Jaeger P, Huisseune H, Van Herzeele S, Vorst N, De Paepe M. Thermo-hydraulic study of a single row heat exchanger consisting of metal foam covered round tubes. Int J Heat and Mass Transfer. 2010; 53(15), 3262–3274.

10. Beavers GS, Sparrow EM. Non-Darcy flow through fibrous porous media. J Appl Mech. 1969;36(4):711–4.

11. Paek JW, Kang BH, Kim SY, Hyun JM. Effective thermal conductivity and permeability of aluminum foam materials. Int J Thermophys. 2000;21(2):453–64.

12. Miwa S, Revankar ST. Hydrodynamic characterization of nickel metal foam, Part 1: Single-phase permeability. Transport Porous Media, 2009; 80(2), 269.

13. Calmidi VV, Mahajan RL. Forced convection in high porosity metal foams. J Heat Transfer. 2000;122(3):557–65.

14. Kim SY, Kang BH, Kim J-H. Forced convection from aluminum foam materials in an asymmetrically heated channel. Int J Heat Mass Transfer. 2001; 44(7), 1451–54.

15. Nazari M, Ashouri M, Kayhani MH, Tamayol A. Experimental study of convective heat transfer of a nanofluid through a pipe filled with metal foam. Int J Thermal Sci. 2015; 88, 33–39.

16. Noh J-S, Lee KB, Lee CG. Pressure loss and forced convective heat transfer in an annulus filled with aluminum foam. Int Commun Heat Mass Transfer. 2006; 33(4), 434–44.

17. Wang H, Guo L. Experimental investigation on pressure drop and heat transfer in metal foam-filled tubes under convective boundary condition. Chem Eng Sci. 2016; 155, 438–48.

18. Mancin S, Zilio C, Rossetto L, Cavallini A. Foam height effects on heat transfer performance of 20 ppi aluminum foams. Appl Thermal Eng. 2012; 49, 55–60.

19. Hamadouche A, Nebbali R, Benahmed H, Kouidri A, Bousri A. Experimental investigation of convective heat transfer in an open-cell aluminum foam. Exp Thermal Fluid Sci. 2016; 71, 86–94.

20. Dukhan N, Patel P. Equivalent particle diameter and length scale for pressure drop in porous metals. Exp Thermal Fluid Sci. 2008; 32(5), 1059–67.

21. Osman S, Sharifpur M, Meyer JP. Experimental investigation of convection heat transfer in the transition flow regime of aluminium oxide-water nanofluids in a rectangular channel. Int J Heat Mass Transfer. 2019; 133, 895–902.

22. Dunn PF. Measurement and Data Analysis for Engineering and Science. 2nd ed. Boca Raton: CRC Press; 2010.

23. Leon T, Roman U. Two-phase gas-liquid flow in rectangular channels. Chem Eng Sci. 1984;39(4):751–65.

24. Poiseuille JLM. Recherches expérimentelles sur le mouvement des liquids dans le tubes detrés petits diamétres. Comptes Rendu. 1840; 11, 961–7, 1041–8, 1840.

25. Blasius PRH. Das Aehnlichkeitsgesetz bei Reibungsvorgangen in Flüssigkeiten. Forschungsheft. 1913;131:1–41.

26. Cengel YA. Heat and Mass Transfer: A Practical Approach 3rd ed. New York, McGraw-Hill; 2007.

27. Tam L-M, Ghajar AJ. Effect of inlet geometry and heating on the fully developed friction factor in the transition region of a horizontal tube. Exp Thermal Fluid Sci. 1997; 15(1), 52–64.

28. Morcos S, Bergles A. Experimental investigation of combined forced and free laminar convection in horizontal tubes. J Heat Transfer. 1975;97(2):212–9.

29. Everts M, Meyer JP. Relationship between pressure drop and heat transfer of developing and fully developed flow in smooth horizontal circular tubes in laminar, transitional, quasi-turbulent and turbulent flow regimes. Int J Heat Mass Transf. 2017;117(2018):1231–50.

30. Olivier JA, Meyer JP. Single-phase heat transfer and pressure drop of the cooling of water inside smooth tubes for transitional flow with different inlet geometries. HVAC and Refrigeration. 2010;16(4):471–96.

31. Gnielinski V. New equations for heat and mass transfer in turbulent pipe and channel flow. Int J Chem Eng. 1979; 16(2), 10.

Publisher's Note